ISSN 1068-3755, Surface Engineering and Applied Electrochemistry, 2021, Vol. 57, No. 5, pp. 595–606. © Allerton Press, Inc., 2021.

Synthesis Characterization and Corrosion Inhibition of Thiourea and Phthalic Anhydride Complex with Ni(II) for Carbon Steel Alloy C1010 0.1 M Hydrochloric Acid

Israa M. Al-Jubanawi[a], Hadi Z. Al-Sawaad[b, *], and Ahmed A. Alwaaly[b, **]

[a] *Mayssan Directorate of Education, Ministry of Education, Bakhdad, Iraq*

[b] *Department of Chemistry, College of Science, University of Basrah, Basra, P.O. Box 49, Iraq*

**e-mail: hadiziara@yahoo.com*

***e-mail: ahmed.alwaaly@me.com*

Received August 16, 2020; revised October 7, 2020; accepted October 9, 2020

Abstract—The research includes synthesis of bis thiourea phthalato nickel (II) complex (PTUNi) by reaction of $NiCl_2 \cdot 6H_2O$ with 2 mol thiourea and 1 mol phthalic anhydride. The (PTUNi) complex was identified by Fourier-transform infrared spectroscopy, UV-visible spectrophotometry, mass spectrophotometry, thermogravimetric differential thermogravimetry analyses, XRD techniques and magnetic susceptibility measurements. The complex was evaluated as corrosion inhibitor for carbon steel alloy (C1010) against a corrosive medium of 0.1 M hydrochloric acid at298 K and showed the maximal efficiency of 95.23% at a concentration of 3 ppm. The effect of temperature on the inhibition behavior was studied at 308, 318 and 328 K and the inhibitor revealed reducing efficiency as temperature raised. The inhibitor behaved as mixed inhibitor. The adsorption of the inhibitor on the surface of the alloy was studied by the Timken, Frumkin, Florry-Hugin and Langmuir adsorption isotherms. The best fitted isotherm was found to be the Langmuir isotherm. The thermodynamic functions like ΔG°_{ads} and ΔH°_{ads} were calculated and revealed that spontaneous adsorption, was exothermic where, the inhibitor was physiochemically adsorbed.

Keywords: thiourea complex, phthalic anhydride, corrosion inhibitor, nickel chloride, nickel complex, carbon steel C1010, acidic medium, tafel plot

DOI: 10.3103/S1068375521050057

INTRODUCTION

Corrosion of metals and alloys is a dangerous problem and it is extradite more attention of corrosion scientists all over the world because of its duplex impacts on both economy and environmental safety [1–4].

Because of the main concerns of corrosion in the durability of materials structure, many studies were always carried out to develop an effective and economic means of corrosion control chosen of an appropriate inhibitor for a certain system may be actually complicated. A corrosion inhibitor adsorbed on the surface of a metal as a protective layer and the strength of the adsorption bond depend on the type of the functional group donor atom, the electron density and the polarizability of the functional group. Corrosion inhibitors normally contain oxygen, sulfur and nitrogen atoms. Multiple bonds in the corrosion inhibitor molecules may facilitate the adsorption on the metal surface [5].

Corrosion inhibition by organic compounds is due to their adsorption on the metal surface to formed protective layers act as insulators between the metal surface and the corrosive medium [6–15].

Such adsorption depends on the nature of the metal, the kind and concentration of the corrosive medium and also on the chemical structure of the inhibitor molecule [14]. Furthermore, adsorption of organic inhibitor on the metal surface depends the functional group, the probable steric effects and electronic density of donor atoms in the inhibitor [16, 17].

Steel alloys are major building materials widely used in broad areas of industrial applications, and almost in everyday life because of their good mechanical properties. However, these steel alloys and other metals and alloys suffer from corrosion phenomena in some environments [18–20]. There are many studies devoted to corrosion inhibitors, the development of corrosion inhibitors was always determined by their effectiveness [21–26].

Thiourea, its compounds and its complexes were used as corrosion inhibitors in industrial operations [27, 28]. In the present work, a novel bis thiourea phthalato nickel(II) (PTUNi) complex was synthe-

Table 1. Elemental composition of C1010 alloy used in this study

Elements	C	Mn	Cr	Cu	S	Si	P	As	Ni	Fe
Content, %	0.13	0.30	0.10	0.30	0.04	0.37	0.05	0.08	0.30	Balance

sized and estimated as corrosion inhibitor against corrosive environment of 0.1 M HCl on the carbon steel C1010 surface.

MATERIALS AND METHODS

The materials utilized in this study were purchase from different companies, including: hydrochloric acid (37 Aldrich), dimethyl sulfoxide (DMSO 99 Alpha), ethanol (99.99 Scharlau), diethylether (99.5 SCH), thiourea (99.99 Aldrich), dichlomethane (99 Fluka), nickel chloride ($NiCl_2{\cdot}6H_2O$ 99.5 GPR), and phthalic anhydride (99.5 GPR).

Preparation of Samples and Test Solution

C1010 type was the carbon steel alloy use in this study. The alloy composition is shown in Table 1 below.

The carbon steel alloy C1010 specimens were strips with length, width, and thickness of 3.1, 1.15 and 0.15 cm, respectively, prepared according to the ASTM G1-72 recommended practice for preparing, washing, and evaluating corrosion test specimens.

A Vernier caliper with a sensitivity of 1 mm was used to calculate the distance. Silicon carbide grades 120, 180, 320, 400, and 600 were used to grind the strips. A specimen was rinsed with cooling water at each stage of the grinding process to minimize the impact of the rise in temperature and to prevent the adhesion of the grinding paper particles, taking into account that each grinding process is perpendicular to the other.

The specimens were then rinsed with water and soap, followed by a wash with distilled water and ethanol to extract the soap residue. Finally, they were polished with acetone and air dried, then polished with a disc rotator covered with alumina Al_2O_3 applied to the polishing disc to make the sample as smooth as a mirror the samples were then rinsed with distilled water, ethanol, and acetone before being air dried. Eventually, to protect the strips from moisture, they were placed in a desiccator.

Synthesis of Bis-Thiourea Phthalato Ni(II) Complex

The following procedure was used to make the PTUNi complex. To begin, dropwise additions of thiourea (6.384 g, 0.084 mol) to a solution of $NiCl_2{\cdot}6H_2O$ (10 g, 0.042 mol) in 100 mL ethanol were made. A solution of phthalic anhydride (6.216 g, 0.042 mol) and sodium hydroxide (3.36 g, 0.084 mol) in 40 mL of water was applied after the solution had been refluxed for around 2 h. For 18 h, the mixture was stirred. After cooling the reaction mixture, the formed green precipitate was filtered and rinsed with distilled water, absolute ethanol, and diethyl ether. The complex was washed by dissolving the solid in a small amount of dichloromethane and then adding a significant amount of ethanol [29]. The solution was left undisturbed at room temperature for 24 h, resulting in a green precipitate that was dried under vacuum. The green substance decomposed at 160–162°C, yielding 9 g, M. Wt.: 374.693 g mol^{-1} (57%) [30, 31]. Scheme 1 shows the synthesis of the complex.

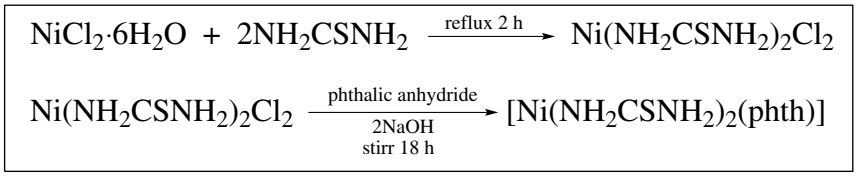

Scheme. 1. Synthesis of PTUNi complex.

The PTUNi complex was characterized by Fourier-transform infrared spectroscopy (FTIR), UV-visible spectrophotomenry, mass spectroscopy, thermogravimentric analysis (TGA) with derivative thermogravimetry (DTG). X-ray diffraction (XRD) techniques, and magnetic susceptibility measurements.

CHNS Elemental Analysis

The CHNS elemental analysis was used to classify the complex PTUNi, which allows for the rapid determination of carbon, hydrogen, nitrogen, and sulfur in organic matrices and other materials.

Table 2 shows matching between theoretical and experimental ratios of CHNS of the complex.

Fourier-Transform Infrared Spectroscopy

The FTIR (KBr pellet, cm^{-1}) spectrum of the complex (Fig. 2) in the region of 400–4000 cm^{-1} shows the following bands: ν_{NH} (3383 cm^{-1}) (assym), 3282 cm^{-1} (sym), $\nu_{C=O}$ (1660 cm^{-1}), ν_{NH} (1558 cm^{-1}) (bending), (1612 cm^{-1}) $\nu_{C=C(aromatic)}$, ν_{COO} (2200), $\nu_{C=S}$(1411), ν_{C-O}(1153), and ν_{CN} (1489), ν_{C-S}(756) and out of plane bending ν_{N-H}(702), ν_{Ni-S} (482 cm^{-1}), and ν_{Ni-O} (655 cm^{-1}) [32–37].

UV-Visible Spectrophotomenry

The complex PTUNi was also characterized by UV-visible spectrophotometry, as shown in Fig. 3, which showed three transitions; 295 nm can be assigned to the benzene ring's $\pi \rightarrow \pi^*$ and $n \rightarrow \pi^*$, as well as the two carboxylic groups in ortho position to one another. For the C=S group, the transition 305 nm is assigned to $n \rightarrow \pi^*$, and 410 nm is assigned to *d–d* transitions [32, 38–40].

Magnetic Susceptibility

The magnetic moment coefficient of a complex was measured and found to be $\mu = 2.0$, magnetic sensitivity calculations confirmed the tetrahedral form and Ni^{+2} nickel oxidation state. The molecular weight, magnetic moment coefficient, oxidation state, and geometry of the complex are shown in Table 3.

Mass Spectroscopy

In addition, mass spectroscopy was used to characterize the complex PTUNi. Figure 4 depicts the mass spectrum of the PTUNi complex, which includes a significant molecular ion peak at 375 *m/z* and a molecular formula $[NiC_{10}H_{12}O_4S_2N_4]^+$, and a peak at 358 *m/z* due to the molecular ion $[NiC_{10}H_9O_4S_2N_3]^+$ after lossing an ammonia molecule. Another peak at 341 *m/z* belongs to the molecular ion $[NiC_{10}H_6O_4S_2N_2]^+$ due to the loss of another ammonia molecule, and the peak at 299 m/z belongs to the molecular ion $[NiC_9H_4O_4S_2]^+$. The peak at 223 *m/z* returns to the molecular ion $[NiC_8H_4O_4]^+$ due to the loss of the CS_2 molecule, and the A peak at 172 *m/z* returns to the molecular ion $[NiC_4HO_4]^+$ due to a loss of the butadiene root HC=CH–CH=CH, which is due to the Durrs reaction that causes the dissociation of the benzene ring. The peak at 104 *m/z* belongs to the molecular ion $[NiCHO_2]^+$ due to the loss of the carbon dioxide molecule CO_2 and the two carbon atoms, and a peak at 76 *m/z* belonging to the molecular ion

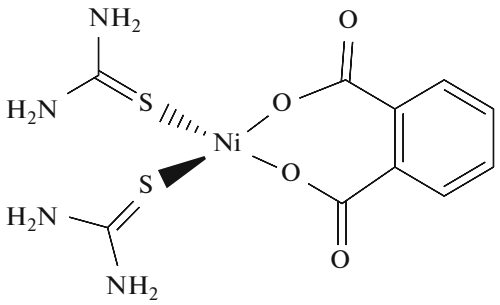

Fig. 1. PTUNi complex.

$[NiOH]^+$ was due to the loss of the carbon monoxide molecule [39].

X-ray Diffraction

The crystal size of the crystallization of the complex was determined using the Debye–Scherer equation borrowed from the XRD diffraction for the diagnosis of PTUNi [32, 37, 41]:

$$D = \frac{K\lambda}{\beta \cos\theta}, \quad (1)$$

where D is the crystallite size (nm), λ is the X-ray wavelength (0.15406 nm for $Cu K_\alpha$), K is the Scherer constant (0.9) that depends on the shape of a crystal, β is the full width at half maximum of intensity, and θ is the Bragg angle, Fig. 5 shows XRD spectrum for PTUNi with a sharp peak at $2\theta = 31.5999°$, $\beta = 0.00872$ radian, and $D = 16.6261$ nm. As it was observed from the crystal size of the crystallized complex, it has the nano structure.

Thermogravimetric with Derivative Thermogravimetry Analysis

Thermal stability of any material is known as the change in the weight of the material as a function of temperature or the change in the weight of the material as a function of time with a constant temperature and can be expressed in several ways.

The geothermal analysis of the complex PTUNi prepared in this study was carried out using thermogravimetric analysis with derivative thermogravimetry (TGA-DTG) technique with a range of temperatures (25–700°C) with a heating rate of 50°C/min in the presence of an inert atmosphere of nitrogen gas, at a flow rate of 30 mL/min. Through this technique,

Table 2. CHNS elemental analysis of PTUNi

$NiC_{12}H_{20}O_4S_4N_8Cl$	C, %	H, %	N, %	S, %
Calculated	32.02	3.20	14.94	17.08
Found	31.55	3.11	14.83	17.04

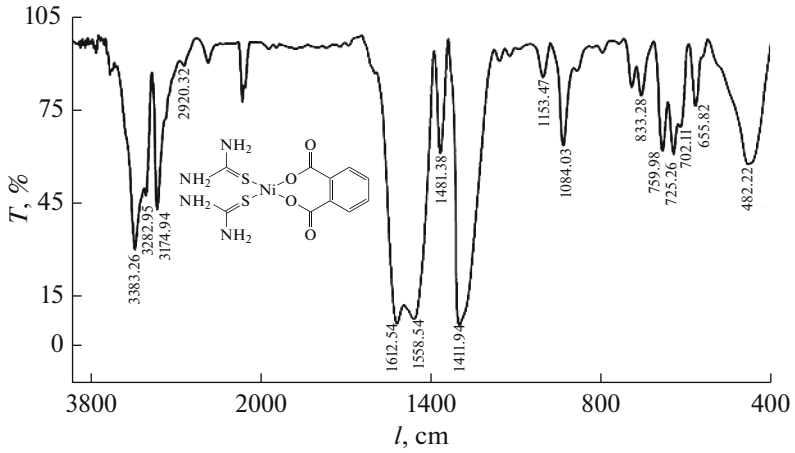

Fig. 2. FTIR spectrum of PTUNi complex.

some thermal functions were calculated, such as the stages of dissociation of the material, the temperature at which the material disintegrates, the dissociation rate, in addition to the remainder after the dissolution process.

In Fig. 6, the TGA and DTG pyrolysis curves show that the complex passed through four dissociation stages.

First stage—at a temperature of 115.55°C, which can be attributed to moisture or solvent residues, the second one—at 236.62°C, the third one—at 276.97°C, and the last one—at 578.69°C.

The value of T_s^* at a temperature of 274°C and the value of the residue at a temperature of 600°C was 62.66%, and the dissociation rate was 2.867%/min. As the follow-up of the disintegration phases, the percentage went down by approximately 38%. The disintegration of two thiourea ligands resulted in the release of nitrogen, carbon, and hydrogen gases [42, 43].

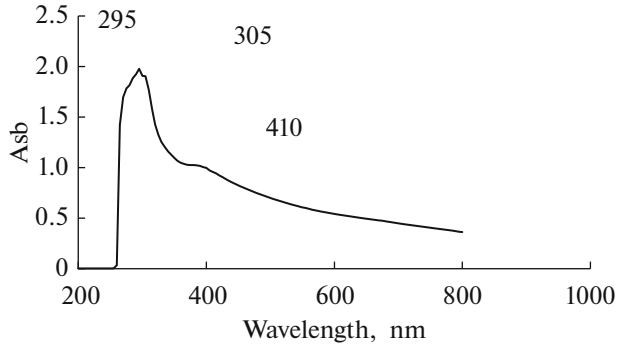

Fig. 3. UV-visible spectrum of PTUNi complex.

Preparation of Working Electrode

In this experiment, a 75 mL vessel was connected to three electrodes: a platinum electrode, a carbon steel specimen, and a saturated calomel electrode, which served as counter, working, and reference electrodes, respectively. Using the electrochemical process, five concentrations of the PTUNi complex (1, 2, 3, 4, and 5 ppm) were prepared to investigate the effect of the complex concentrations on the corrosion of the C1010 alloy surface at 298 K (Tafel plot method). The effect of temperature on the corrosion reaction in the presence and the absence of both the optimal and the maximal PTUNi concentrations was studied at 298, 308, 318, and 328 K in 0.1 M HCl as corrosive agent.

RESULTS AND DISCUSSION

Figure 7 show Tafel plots for five concentrations of the PTUNi complex relative to blank in 0.1 M HCl.

The electrochemical data were summarized in Table 4 below.

As the Table 4 above shows, the inhibition efficiency (*IE%*) is 95.23% at a concentration of 3 ppm, i.e., it is the optimal concentration, and the efficiency was calculated by the following equation as borrowed from [44]:

$$IE\% = \frac{CR_{\text{uninhib}} - CR_{\text{inhib}}}{CR_{\text{uninhib}}} \times 100, \qquad (2)$$

where CR_{uninhib} and CR_{inhib} are the corrosion rates of the C1010 alloy in the absence and the presence of the inhibitor, respectively. As in Table 4, no significant difference in the inhibition efficiency at higher concentrations of the inhibitor were registered, which means that the inhibitor tends to be well adsorbed at all these five concentrations, with those of 3 and 5 ppm being considered as the optimal and the minimal concentrations, respectively.

Table 4 shows that the presence of the complex PTUNi lowered the corrosion rate of the surface of the C1010 alloy at all concentrations as compared to the blank HCl solution because the corrosion current density decreased and the resistance polarization of the alloy increased [45, 46].

The corrosion current in the presence of the inhibitor decreased to 32.18 μA cm^{-2} and the corrosion rate to 14.90 mpy. At the optimum concentration of 3 ppm, the inhibition efficiency of 95.23% was the highest; the area of the layer covering the surface of the alloy with the inhibitor $\theta = 0.9523$, too, and the polarization resistance of the alloy in the presence of this inhibitor reached 559.28 Ω cm^2 compared to the respective values in the corrosive medium without the inhibitor. An increase in the inhibitor concentration causes a slight increase in the inhibition efficiency to the optimal concentration of 3 ppm, and then the value decreases by a small amount, and the area covered by the inhibitor becomes the lowest ($\theta = 0.9142$) since the inhibition efficiency became also the lowest (91.42%).

The spatial shape of the complex PTUNi is to blame for a small decrease in the values of inhibition efficiency in the presence of this inhibitor. E_{corr} values changed by less than 89 mV as compared to the null, indicating that the inhibitor analyzed here is a mixed inhibitor [47, 48]; since both β_a and β_c values shifted compared with those in the blank specimen, it can be concluded that the anodic dissolution in the anode and the hydrogen evolution in the cathode were controlled [49]. Figure 8 explained the relation between these data and the concentrations of the inhibitor.

Table 3. Magnetic susceptibility of PTUNi complex

Complex	M. Wt.	μ_{eff}	Shape	Oxidation state
PTUNi	374.69	2.0	Tetrahedral	+2

Adsorption Behavior of PTUNi Complex on C1010 Surface

The effect of the adsorption film for the described complex on the surface of the mentioned alloy was investigated using various adsorption isotherms such as the Langmuir, Freundlich, Timken, Florry-Hugin, and Frumkin ones. The Langmuir adsorption isotherm best suit the experimental results. Equation (3) (borrowed from) is the equation that gives a regression coefficient R^2 near unity [50–53]:

$$\frac{c}{\theta} = \frac{1}{K_{ads}} + C, \quad (3)$$

where C is the molar concentration of PTUNi, K_{ads} is the equilibrium constant of adsorption, and θ is the surface coverage area by the inhibitor calculated according to Eq. (4) as borrowed from [44]:

$$\theta = \frac{CR_{uninhib} - CR_{inhib}}{CR_{uninhib}}. \quad (4)$$

Figure 9 shows the Langmuir adsorption isotherm where the equilibrium constant was calculated from the intercept of Eq. (3):

Thus, the standard free energy of adsorption ΔG°_{ads} in kJ mol^{-1} can be calculated depending upon the equilbrium constant of adsorption according to Eq. (5) as borrowed from [52–54]:

$$\Delta G^{\circ}_{ads} = -RT \ln 55.5 K_{ads}, \quad (5)$$

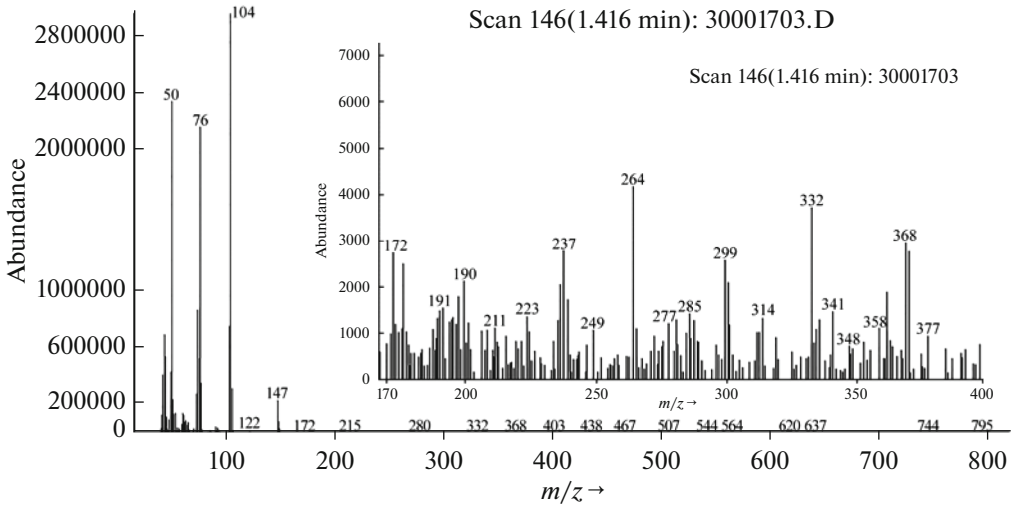

Fig. 4. Mass spectrum of PTUNi complex.

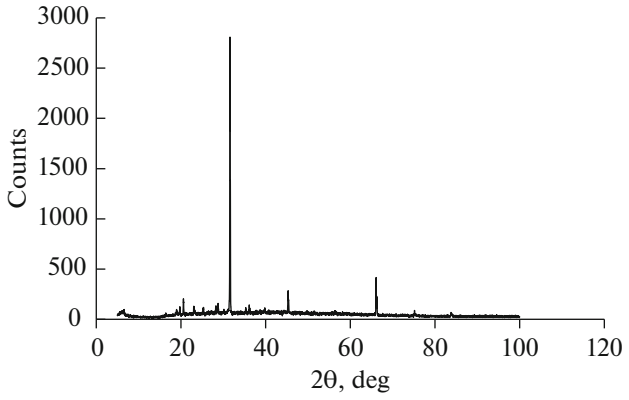

Fig. 5. XRD spectrum of PTUNi complex.

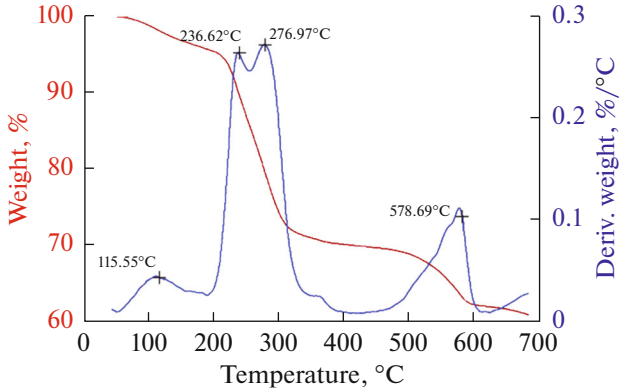

Fig. 6. TGA and DTG pyrolysis curves.

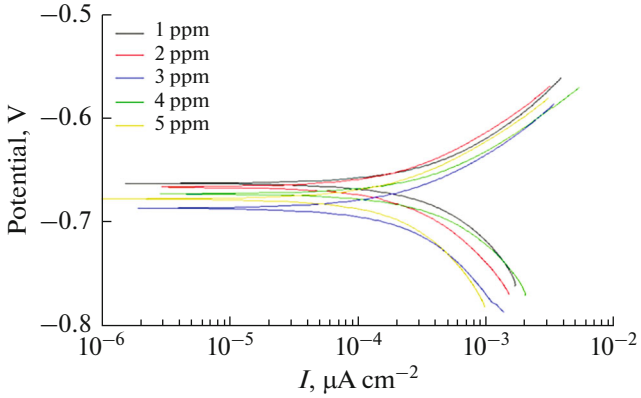

Fig. 7. Tafel plots for carbon steel alloy C1010 in presence of different concentrations of PTUNi complex at 298K.

where R is the universal gas equal to 8.314 J K^{-1} mol^{-1}. T is the absolute temperature in K, and the value 55.5 is the molar concentration of the water molecules in the corrosive medium. In addition, the standard enthalpy of adsorption ΔH°_{ads} in kJ mol^{-1} is calculated according to the Van't Hoff equation (Eq. (6) below) as borrowed from [43]:

$$\ln K_{ads} = \text{constant} - \left(\frac{\Delta H^{\circ}_{ads}}{R}\right)\frac{1}{T}, \qquad (6)$$

where K_{ads} was calculated for 3 and 5 ppm as the optimal and maximal concentratios i.e., the concentration with higher and lower inhibition effeciency respectively. Figures 10 and 11 showed the plotting of the relationship between $\ln K_{ads}$ against $\frac{1}{T}$ to give the straight line with slope equal to $\left(\frac{-\Delta H^{\circ}_{ads}}{R}\right)$.

All thermodynamic functions were summarized in Table 5 below.

Table 5 shows that as the temperature rose, the adsorption equilibrium constant decreased, indicating that the process was by desorption rather than adsorption. At all temperatures, the adsorption process was spontaneous, but it slowed as the temperature rose.

Adsorption is physisorption if the value is less than 40.0 kJ mol^{-1}, but chemisorption if the value is greater than 100.0 kJ mol^{-1} [56–58]. Since the emulsion adsorption values are in the middle of those two ranges. The adsorption of the inhibitor under investigation is a combination of chemical and physical adsorptions, with a higher proportion of chemical adsorption. The negative adsorption free energy values ΔG°_{ads} indicate that the adsorption mechanism is automatic (spontaneous) [59]. In other words, the inhibitor appears to be adsorbed on the alloy surface, forming an adsorbent layer that inhibits corrosion. At the optimum concentration of PTUNi, the adsorption equilibrium constant K_{ads} increases at higher temperatures and decreases at its maximal concentration.

Also, the value of the enthalpy adsorption of the PTUNi complex at the optimum concentration is noted to be $R^2 = 0.3441$ due to the stability of the value of the damping efficiency at the first three temperatures, and then there is a significant drop in the damping efficiency at 328 K.

Study of Effect of Temperature on Corrosion Rate of C1010 Alloy

The effect of temperature on the corrosion reaction on the surface of the mentioned alloy was studied at 298, 308, 318, and 328 K by using Tafel plots at the optimal concentration (3 ppm) and at the maximal one (5 ppm) as in Figs. 12, 13, and 14. Thus, an electrochemical data for both cases were obtained and summerized in Tabel 6.

As shown in Table 6, The PTUNi complex works best at a concentration of 3 ppm, and the inhibitor can keep its inhibition efficiency between 298 and 318 K.

Table 4. At 298K, electrochemical data for corrosion of the C1010 alloy surface in the presence of various concentrations of PTUNi compared to a void

Comp.	Conc., ppm	E_{corr}, mV	β_a, mV	β_c, mV	R_p, Ω cm^2	I_{corr}, μA cm^{-2}	*CR*, mpy	*IE%*	θ
HCl	3650	–659	171.27	–333.06	26.28	685.06	317.23	–	–
PTUNi	1	–686	237.2	–214.33	513.5	35.05	16.23	94.82	0.9482
	2	–667	307.6	–251.29	492.07	36.58	16.94	94.59	0.9459
	3	–700	251.29	–226.06	559.28	32.18	14.90	95.23	0.9523
	4	–671	480.41	–484.6	366.51	49.11	22.74	92.76	0.9276
	5	–704	597.51	–1001.3	308.64	58.32	27.00	91.42	0.9142

Table 5. Standard thermodynamic functions for adsorption of the PTUNi inhibitor on the surface of C1010 alloy

Comp.	$C \times 10^{-6}$, mol L^{-1}	Temp., K	$K_{ads} \times 10^6$, L mol^{-1}	ΔG°_{ads}, kJ mol^{-1}	ΔH°_{ads}, kJ mol^{-1}	R^2
PTUNi	8.01	298	2.49	–46.44	–48.72	0.3441
PTUNi		308	2.51	–48.02		
PTUNi		318	2.97	–50.02		
PTUNi		328	0.19	–44.10		
PTUNi	13.4	298	0.80	–43.63	–75.00	0.9390
PTUNi		308	0.27	–42.31		
PTUNi		318	0.11	–41.31		
PTUNi		328	0.07	–41.38		

As the temperature reaches 328 K, the damping's performance plummets, as it is observed that the values of the corrosion rate and the corrosion current at the mentioned temperatures are close, but the values of the corrosion rate changed from 14.90 to 350.85 mpy and pf the corrosion current from 32.18 to 757.60 μA cm^{-2}, and the polarization resistance decreased from 559.28 to 23.75 Ω cm^2 when the temperature rises from 298 to 328 K. At the biggest concentration, the decrease is evident and regular.

As the rate of corrosion and the corrosion current have increased their values within this range of temperatures from (27) mpy, (58.32) μA cm^{-2} to (460.73) mpy, (994.92) μA cm^{-2} in presence of 5 ppm of the inhibitor. The polarization resistance has decreased from 308.64 to 18.09 Ω cm^2, also the damper has dual behavior in the optimum and highest concentrations in spite of the high temperature, but in the case of the optimal concentration, the values of the anode and cathode indicate the maintenance of control over the

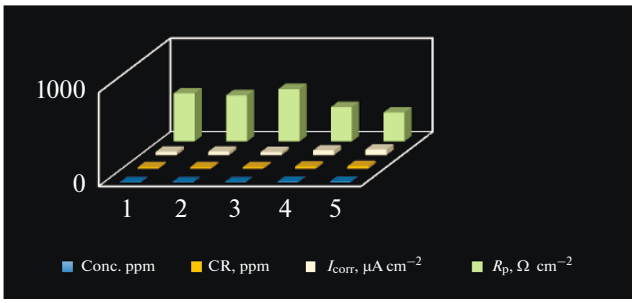

Fig. 8. Relation between inhibitor concentration and electrochemical data for C1010 surface.

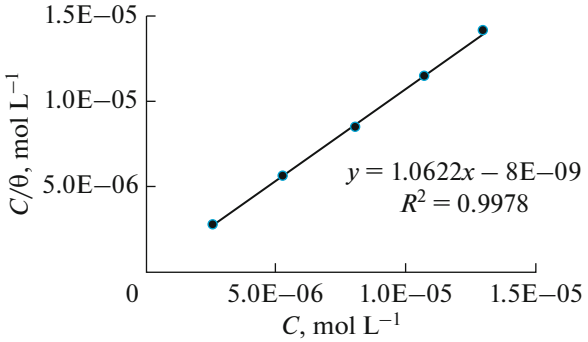

Fig. 9. Langmuir adsorption isotherm for PTUNi on C1010 surface.

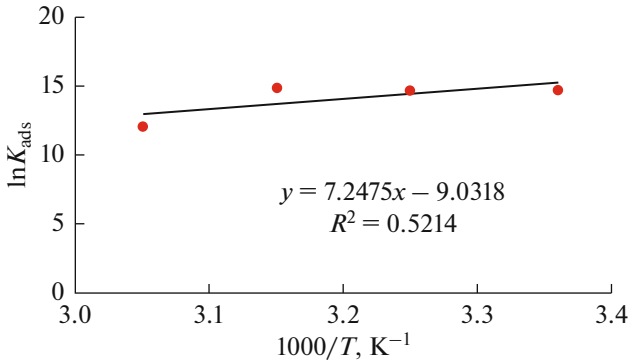

Fig. 10. Calculation of standard enthalpy of adsorption of 3 ppm (optimal conc.) of PTUNi on C1010 surface by Van't Hoff equation.

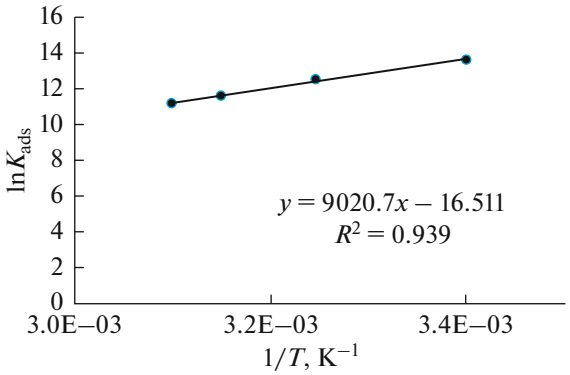

Fig. 11. Calculation of standard enthalpy of adsorption of 5 ppm (maximal conc.) of PTUNi on C1010 surface by Van't Hoff equation.

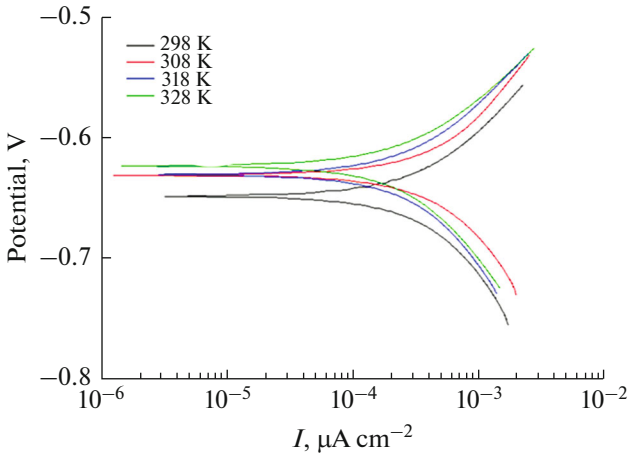

Fig. 12. Tafel plots for C1010 in presence of corrosive environment of 0.10 M HCl at different temperatures.

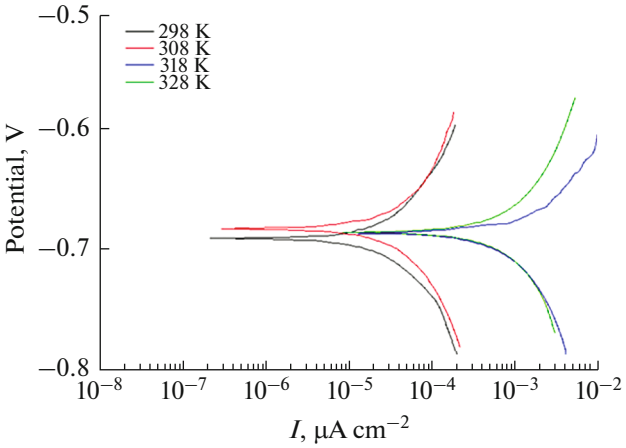

Fig. 13. Tafel plots for C1010 in presence of optimal concentration (3 ppm) of PTUNi at different temperatures.

Table 6. Electrochemical evidence for corrosion of C1010 surfaces in the presence of optimal (3 ppm) and maximum (5 ppm) PTUNi concentrations at various temperatures relative to the blank (3650 ppm)

Comp.	Conc., ppm	Temp., K	E_{corr}, mV	β_a, mV	β_c, mV	R_{ct}, Ω cm^2	I_{corr}, μA Cm^{-2}	CR, mpy	*IE%*	θ
HCl	3650	298	–659	171.27	–333.06	26.28	685.06	317.23	–	
HCl		308	–670	370.54	–825.15	21.86	823.32	381.26	–	
HCl		318	–674	56.45	–186.37	15.87	1132.1	525.16	–	
HCl		328	–678	193.53	–1165.40	9.41	1912.3	885.45	–	
PTUNi	3	298	–700	251.29	–226.06	559.28	32.18	14.90	95.23	0.9523
PTUNi	3	308	–691	421.88	–329.11	471.09	38.20	17.69	95.26	0.9526
PTUNi	3	318	–690	613.31	–349.93	412.42	43.64	20.21	95.96	0.9596
PTUNi	3	328	–695	331.60	–454.13	23.75	757.60	350.85	60.41	0.6041
PTUNi	5	298	–704	597.51	–1001.3	308.64	58.32	27.00	91.42	0.9142
PTUNi	5	308	–712	351.99	–372.38	101.43	177.46	82.18	78.36	0.7836
PTUNi	5	318	–702	332.81	–341.39	39.69	453.50	210.00	59.88	0.5988
PTUNi	5	328	–694	116.97	–210.84	18.09	994.92	460.73	47.99	0.4799

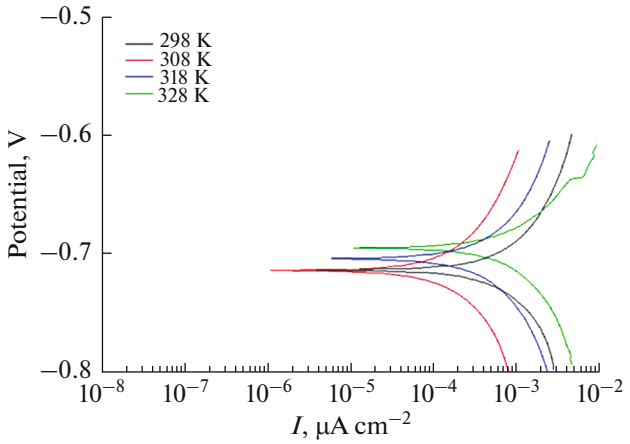

Fig. 14. Tafel plots for C1010 in presence of maximal concentration (5 ppm) of PTUNi at different temperatures.

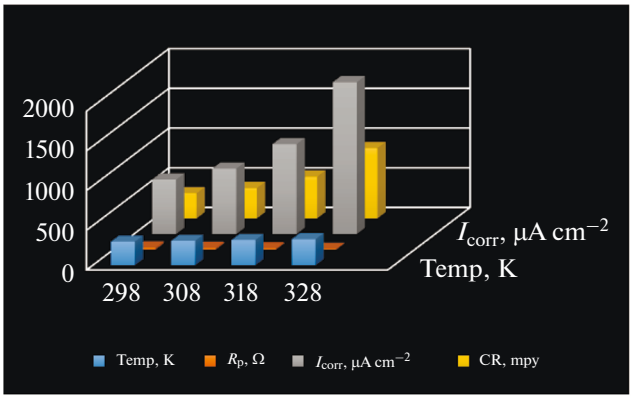

Fig. 15. Effect of temperature on electrochemical parameters of C1010 in absence of inhibitor.

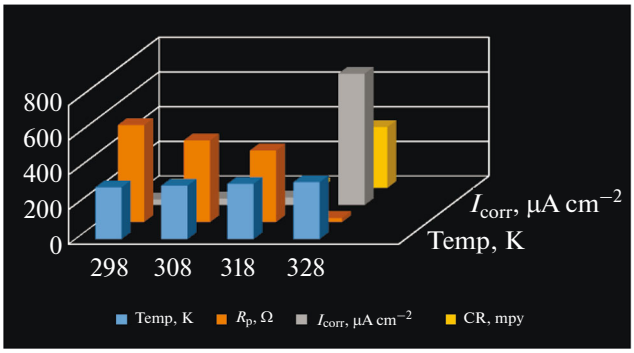

Fig. 16. Effect of temperature on electrochemical parameters of C1010 alloy in presence of optimal concentration (3 ppm).

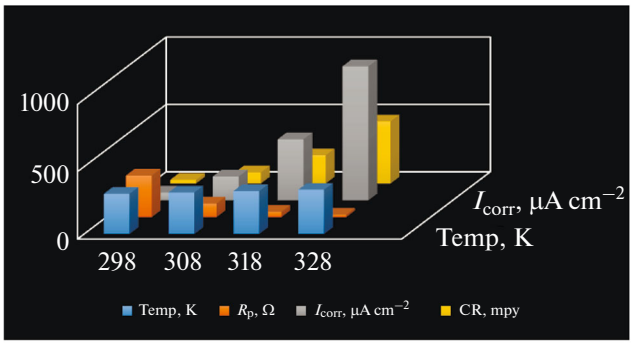

Fig. 17. Effect of temperature on electrochemical parameters of C1010 in presence of maximal concentration (5 ppm) of PTUNi.

anode and cathode reaction mechanisms up to 328 K, unlike in the case of the higher concentration, then these values decrease, which indicates a loss of control over the two reactions mentioned [55]. In comparison to the decrease in *IE%* at the optimum concentration with rising temperature within the aforementioned thermal range, a substantial decrease is also observed.

As a result, using the ideal PTUNi concentration of 3 ppm is preferred. The values of the Tafel anode and cathode constants are changing in both cases, and there is a decrease, indicating a reduction in the control mechanisms of the anode and cathode reactions [45, 60]. In Figs. 15, 16 and 17 the effect of temperature on the corrosion rate and other electrochemical parameters is shown.

CONCLUSIONS

(1) The nickel complex PTUNi has a tetrahedral geometrical shape and is paramagnetic, which confirms the replacement of two ligands from thiourea versus one ligand of phthalates.

(2) The nickel complex PTUNi can be used as corrosion inhibitor for corrosive environment of 0.1 M of HCl at a quite low concentration, i.e., 3 ppm, with the efficiency of 95.23%; and it behaves as mixed inhibitor.

(3) The inhibitor PTUNi raised the activation energy for the corrosion reaction on the surface of C1010 alloy.

(4) The mechanism of hydrogen evolution in the cathode and anodic dissolution can be controlled in the presence of this inhibitor.

CONFLICT OF INTEREST

The authors declare that they have no conflict of interest.

REFERENCES

1. El-Lateef, H.M.A., Adam, M.S.S., and Khalaf, M.M., Synthesis of polar unique 3D metal-imine complexes of salicylidene anthranilate sodium salt. Homogeneous catalytic and corrosion inhibition performance, *J. Taiwan Inst. Chem. Eng.*, 2018, vol. 88, p. 286.

2. Kadhima, Z.N., Mahadia, M.A., and Al-Sawaada, H.Z., Synthesis, characterization and corrosion inhibitors evaluation of some Schiff base complexes of copper(II), and molybdenum(VI), *Int. J. Acad. Stud.*, 2016, vol. 2, no. 11, p. 446.

3. Goyal, M., Kumar, S., Bahadur, I., Verma, C., et al., Organic corrosion inhibitors for industrial cleaning of ferrous and non-ferrous metals in acidic solutions: A review, *J. Mol. Liq.*, 2018, vol. 256, p. 565.

4. Liu, X., Okafor, P.C., Jiang, B., Hu, H., et al., Electrochemical study on the inhibition effect of phenanthroline and its cobalt complex as corrosion inhibitors for mild steel, *J. Mater. Eng. Perform.*, 2015, vol. 24, no. 9, p. 3599.

5. Alwan, W.M., Synthesis, characterization and the corrosion inhibition study of two Schiff base ligands derived from urea and thiourea and their complexes with Cu(II) and Hg(II) ions, *J. Phys.: Conf. Ser.*, 2018, vol. 1003, no. 1, art. ID 012017. https://doi.org/10.1088/1742-6596/1003/1/012017

6. Fawzy, A., Zaafarany, I.A., Ali, H.M., and Abdallah, M., New synthesized amino acids-based surfactants as efficient inhibitors for corrosion of mild steel in hydrochloric acid medium: Kinetics and thermodynamic approach, *Int. J. Electrochem. Sci.*, 2018, vol. 13, no. 5, p. 4575.

7. Fawzy, A., Abdallah, M., Zaafarany, I.A., Ahmed, S.A., et al., Thermodynamic, kinetic and mechanistic approach to the corrosion inhibition of carbon steel by new synthesized amino acids-based surfactants as green inhibitors in neutral and alkaline aqueous media, *J. Mol. Liq.*, 2018, vol. 265, p. 276.

8. Abdallah, M., Hazazi, O.A., Fawzy, A., El-Shafei, S., et al., Influence of N-thiazolyl-2-cyanoacetamide derivatives on the corrosion of aluminum in 0.01 M sodium hydroxide, *Prot. Met. Phys. Chem. Surf.*, 2014, vol. 50, no. 5, p. 659.

9. Awad, M., Saad, A.F., Shaaban, M.R., AL Jahdaly, B.A., et al., New insight into the mechanism of the inhibition of corrosion of mild steel by some amino acids, *Int. J. Electrochem. Sci.*, 2017, vol. 12, p. 1657.

10. Hazazi, O.A., Fawzy, A., Shaaban, M.R., and Awad, I.M., Enhanced 4-amino-5-methyl-4*H*-1,2,4-triazole-3-thiol inhibition of corrosion of mild steel in 0.5 M H_2SO_4 by Cu(II), *Int. J. Electrochem. Sci.*, 2014, vol. 9, p. 1378.

11. Takroni, K.M., El-Ghamry, H.A., and Fawzy, A., Evaluation of the catalytic activities of some synthesized divalent and trivalent metal complexes and their inhibition efficiencies for the corrosion of mild steel in sulfuric acid medium, *J. Inorg. Organomet. Polym. Mater.*, 2019, vol. 29, no. 6, p. 1927.

12. Biswas, A., Das, D., Lgaz, H., Pal, S., et al., Biopolymer dextrin and poly (vinyl acetate) based graft copolymer as an efficient corrosion inhibitor for mild steel in hydrochloric acid: electrochemical, surface morphological and theoretical studies, *J. Mol. Liq.*, 2019, vol. 275, p. 867.

13. Abdallah, M., Fouda, A.S., Zaafarany, I., Fawzy, A., et al., Corrosion inhibition of iron in sulphuric acid solution by antibacterial cephalosporin, *J. Am. Sci.*, 2013, vol. 9, no. 3, p. 209.

14. Bentiss, F., Lagrenee, M., Traisnel, M., and Hornez, J.C., The corrosion inhibition of mild steel in acidic media by a new triazole derivative, *Corros. Sci.*, 1999, vol. 41, no. 4, p. 789.

15. Hazazi, O., Fawzy, A., and Awad, M., Synergistic effect of halides on the corrosion inhibition of mild steel in H_2SO_4 by a triazole derivative: Kinetics and thermodynamic studies, *Int. J. Electrochem. Sci.*, 2014, vol. 9, p. 4086.

16. Bentiss, F., Lagrenée, M., and Traisnel, M., 2,5-Bis(*n*-pyridyl)-1,3,4-oxadiazoles as corrosion inhibitors for mild steel in acidic media, *Corrosion*, 2000, vol. 56, no. 7, p. 733.

17. Abdallah, M., AL Jahdaly, B.A., Salem, M.M., Fawzy, A., et al., Electrochemical behavior of nickel alloys and stainless steel in HNO_3 using cyclic voltammetry technique, *J. Mater. Environ. Sci.*, 2017, vol. 8, p. 1320.

18. Fuchs-Godec, R. and Pavlović, M.G., Synergistic effect between non-ionic surfactant and halide ions in the forms of inorganic or organic salts for the corrosion inhibition of stainless-steel X4Cr13 in sulphuric acid, *Corros. Sci.*, 2012, vol. 58, p. 192.

19. Abdallah, M., Zaafarany, I., Fawzy, A., Radwan, M.A., et al., Inhibition of aluminum corrosion in hydrochloric acid by cellulose and chitosan, *J. Am. Sci.*, 2013, vol. 9, p. 580.

20. Hazazi, O.A., Fawzy, A., and Awad, M.I., Sulfachloropyridazine as an eco-friendly inhibitor for corrosion of mild steel in H_2SO_4 solution, *Chem. Sci. Rev. Lett.*, 2015, vol. 4, p. 67.

21. ELouadi, Y., Abrigach, F., Bouyanzer, A., and Touzani, R., Corrosion inhibition of mild steel by new N-heterocyclic compound in 1 M HCl: Experimental and computational study, *Pharma Chem.*, 2015, vol. 7, no. 8, p. 265.

22. Cherrak, K., Dafali, A., Elyoussfi, A., El Ouadi, Y., et al., Two new benzothiazine derivatives as corrosion inhibitors for mild steel in hydrochloric acid medium, *J. Mater. Environ. Sci.*, 2017, vol. 8, no. 2, p. 636.

23. El Ouadi, Y., Elmsellem, H., El Fal, M., Sebbar, N.K., et al., Effect of 1,5-di(prop-2-ynyl)-1*H*-pyrazolo[3,4-d]pyrimidine-4(5*H*)-thione on inhibition of mild steel corrosion in 1 M HCl, *Pharma Chem.*, 2016, vol. 8, no. 1, p. 365.

24. Bader, A., Shaheen, U., Aborehab, M.A.S., El Ouadi, Y., et al., Inhibitory effect of *Acacia hamulosa* methanolic extract on the corrosion of mild steel, in 1 M hydrochloric acid, *Bull. Chem. Soc. Ethiop.*, 2018, vol. 32, no. 2, p. 323.

25. Merimi, I., El Ouadi, Y., Ansari, K.R., Oudda, H., et al., Adsorption and corrosion inhibition of mild steel by ((*Z*)-4-((2,4-dihydroxybenzylidene)amino)-5-methy-2,4 dihydro-3*H*-1,2,4-triazole-3-thione) in 1 M HCl: Experimental and computational study, *Anal. Bioanal. Electrochem.*, 2017, vol. 9, no. 5, p. 640.

26. Merimi, I., El Ouadi, Y., Benkaddour, R., Lgaz, H., et al., Improving corrosion inhibition potentials using two triazole derivatives for mild steel in acidic medium: experimental and theoretical studies, *Mater. Today: Proc.*, 2019, vol. 13, p. 920.

27. Shen, C., Wang, S.G., Yang, H.Y., Long, K., et al., Corrosion and corrosion inhibition by thiourea of bulk

nanocrystallized industrial pure iron in dilute HCl solution, *Corros. Sci.*, 2006, vol. 48, no. 7, p. 1655.

28. Huong, D.Q., Duong, T., and Nam, P.C., Effect of the structure and temperature on corrosion inhibition of thiourea derivatives in 1.0 M HCl solution, *ACS Omega*, 2019, vol. 4, no. 11, p. 14478.
29. Ajibade, P.A. and Zulu, N.H., Metal complexes of diisopropylthiourea: synthesis, characterization and antibacterial studies, *Int. J. Mol. Sci.*, 2011, vol. 12, no. 10, p. 7186.
30. Binzet, G., Kavak, G., Külcü, N., Özbey, S., Flörke, U., and Arslan, H., Synthesis and characterization of novel thiourea derivatives and their nickel and copper complexes, *J. Chem.*, 2013, vol. 2013, art. ID 536562. https://doi.org/10.1155/2013/536562
31. Halim, N.I.M., Kassim, K., Fadzil, A.H., and Yamin, B.M., Sintesis, pencirian dan kajian aktiviti antibakteria kompleks Cu(II) tiourea, *Malays. J. Anal. Sci.*, 2012, vol. 16, no. 1, p. 56.
32. Larouj, M., Ourrak, K., El M'Rabet, M., Zarrok, H., et al., Thermodynamic study of corrosion inhibition of carbon steel in acidic solution by new pyrimidothiazine derivative, *J. Mater. Environ. Sci.*, 2017, vol. 8, no. 11, p. 3921.
33. Devika, B., Doreswamy, B., and Tandon, H., Corrosion behaviour of metal complexes of antipyrine based azo dye ligand for soft-cast steel in 1 M hydrochloric acid, *J. King Saud Univ. Sci.*, 2020, vol. 32, no. 1, p. 881.
34. Fernandes, C.M., Alvarez, L.X., dos Santos, N.E., Barrios, A.C.M., et al., Green synthesis of 1-benzyl-4-phenyl-1*H*-1,2,3-triazole, its application as corrosion inhibitor for mild steel in acidic medium and new approach of classical electrochemical analyses, *Corros. Sci.*, 2019, vol. 149, p. 185.
35. Manssouri, M., El Ouadi, Y., Znini, M., Costa, J., et al., Adsorption proprieties and inhibition of mild steel corrosion in HCl solution by the essential oil from fruit of Moroccan *Ammodaucus leucotrichus, J. Mater. Environ. Sci.*, 2015, vol. 6, no. 3, p. 631.
36. Radey, H.H., Khalaf, M.N., and Al-Sawaad, H.Z., Novel corrosion inhibitors for carbon steel alloy in acidic medium of 1 N HCl synthesized from graphene oxide, *Open J. Org. Polym. Mater.*, 2018, vol. 8, no. 04, p. 53.
37. AL-Sawaad, H.Z., Evaluation of the ceftriaxone as corrosion inhibitor for carbon steel alloy in 0.5 M of hydrochloric acid, *Int. J. Electrochem. Sci.*, 2013, 8, p. 3105.
38. Fouda, A., El-morsi, M.A., Gaber, M., and Fakeeh, M., A comparative study of the corrosion inhibition of carbon steel in HCl solution by 1-[(5-mercapto-1*H*-1,2,4-triazole-3-yl) diazenyl] naphthalene-2-ol (HL) and its manganese complex, *Chem. Data Collect.*, 2020, vol. 28, art. ID 100479.
39. Fateh, A., Aliofkhazraei, M., and Rezvanian, A., Review of corrosive environments for copper and its corrosion inhibitors, *Arab. J. Chem.*, 2020, vol. 13, no. 1, p. 481.
40. El Aoufir, Y., Aslam, R., Lazrak, F., Marzouki, R., et al., The effect of the alkyl chain length on corrosion inhibition performances of 1,2,4-triazole-based compounds for mild steel in 1.0 M HCl: Insights from experimental and theoretical studies, *J. Mol. Liq.*, 2020, vol. 303, art. ID 112631.
41. Hsissou, R., Benhiba, F., About, S., Dagdag, O., et al., Trifunctional epoxy polymer as corrosion inhibition material for carbon steel in 1.0 M HCl: MD simulations, DFT and complexation computations, *Inorg. Chem. Commun.*, 2020, vol. 115, art. ID 107858. https://doi.org/10.1016/j.inoche.2020.107858
42. Ardakani, E.K., Kowsari, E., and Ehsani, A., Imidazolium-derived polymeric ionic liquid as a green inhibitor for corrosion inhibition of mild steel in 1.0 M HCl: experimental and computational study, *Colloids Surf., A*, 2020, vol. 586, art. ID 124195.
43. Lebrini, M., Robert, F., and Roos, C., Adsorption properties and inhibition of C38 steel corrosion in hydrochloric solution by some indole derivates: temperature effect, activation energies, and thermodynamics of adsorption, *Int. J. Corros.*, 2013, vol. 2013, art. ID 139798. https://doi.org/10.1155/2013/139798
44. AL-Jubanawi, I.M., AL-Sawaad, H.Z., and AL-Waaly, A.A., Bis thiourea phthalato cobalt(II) complex: synthesis and studying as corrosion inhibitors for carbon steel alloy (C1010) in 0.1 M HCl, *J. Mater. Environ. Sci.*, 2020, vol. 11, p. 1386.
45. El-Lateef, H.M.A., El-Sayed, A.R., Mohran, H.S., and Shilkamy, H.A.S., Corrosion inhibition and adsorption behavior of phytic acid on Pb and Pb–In alloy surfaces in acidic chloride solution, *Int. J. Ind. Chem.*, 2019, vol. 10, no. 1, p. 31.
46. Shukla, S.K. and Ebenso, E.E., Corrosion inhibition, adsorption behavior and thermodynamic properties of streptomycin on mild steel in hydrochloric acid medium, *Int. J. Electrochem. Sci.*, 2011, vol. 6, no. 8, p. 3277.
47. El-Tabesh, R., Abdel-Gaber, A.M., Hammud, H., and Oweini, R., Effect of mixed-ligands copper complex on the corrosion inhibition of carbon steel in sulfuric acid solution, *J. Bio- Tribo-Corros.*, 2020, vol. 6, no. 2, p. 29.
48. Al-Sawaad, H.Z., Faili, N.T., and Essa, A.H., Evaluation of vicine as a corrosion inhibitor for carbon steel alloy, *Port. Electrochim. Acta*, 2019, vol. 37, no. 4. p. 205.
49. El-Gammal, O.A., Fouda, A.E.-A.S., and Nabih, D.M., Novel Mn^{2+}, Fe^{3+}, Co^{2+}, Ni^{2+} and Cu^{2+} complexes of potential OS donor thiosemicarbazide: design, structural elucidation, anticorrosion potential study and antibacterial activity, *J. Mol. Struct.*, 2020, vol. 1204, art. ID 127495.
50. Rao, C., Venkataraghavan, R., and Kasturi, T., Contribution to the infrared spectra of organosulphur compounds, *Can. J. Chem.*, 1964, vol. 42, no. 1, p. 36.
51. Zakaria, S.A., Muharam, S.H., Yusof, M.S.M., Khairul, W.M., et al., Spectroscopic and structural study of a series of pivaloylthiourea derivatives, *Malays. J. Anal. Sci.*, 2011, vol. 15, no. 1, p. 37.
52. Akpomie, K.G., Fayomi, O.M., Ezeofor, C.C., Sha'Ato, R., et al., Insights into the use of metal complexes of thiourea derivatives as highly efficient adsorbents for ciprofloxacin from contaminated water, *Trans. R. Soc. South Afr.*, 2019, vol. 74, no. 2, p. 180.
53. Sonmez, M., Synthesis and characterization of copper(II), nickel(II), cadmium(II), cobalt(II) and zinc(II) complexes with 2-benzoyl-3-hydroxy-1-naph-

thylamino-3-phenyl-2-propen-1-on, *Turk. J. Chem.*, 2001, vol. 25, no. 2, p. 181.

54. Ibrahim, O.B., Complexes of urea with Mn(II), Fe(III), Co(II), and Cu(II) metal ions, *Adv. Appl. Sci. Res.*, 2012, vol. 3, no. 6, p. 18.
55. Ghazal, K., Shoaib, S., Khan, M., Khan, S., et al., Synthesis, characterization, X-ray diffraction study, in-vitro cytotoxicity, antibacterial and antifungal activities of nickel(II) and copper(II) complexes with acyl thiourea ligand, *J. Mol. Struct.*, 2019, vol. 1177, p. 124.
56. Refat, M.S., El-Deen, I.M., Zein, M.A., Adam, A.M., et al., Spectroscopic, structural and electrical conductivity studies of Co(II), Ni(II) and Cu(II) complexes derived from 4-acetylpyridine with thiosemicarbazide, *Int. J. Electrochem. Sci.*, 2013, vol. 8, no. 7, p. 9894.
57. Tan, S.S., Al-Abbasi, A.A., Tahir, M.I.M., and Kassim, M.B., Synthesis, structure and spectroscopic properties of cobalt(III) complexes with 1-benzoyl-(3,3-disubstituted)thiourea, *Polyhedron*, 2014, vol. 68, p. 287.
58. Monshi, A., Foroughi, M.R., and Monshi, M.R., Modified Scherrer equation to estimate more accurately nano-crystallite size using XRD, *World J. Nano Sci. Eng.*, 2012, vol. 2, no. 3, p. 154.
59. Breviglieri, S.T., Cavalheiro, E.T.G., and Chierice, G.O., Correlation between ionic radius and thermal decomposition of Fe(II), Co(II), Ni(II), Cu(II) and Zn(II) diethanoldithiocarbamates, *Thermochim. Acta*, 2000, vol. 356, nos. 1–2, p. 79.
60. El-Sawaf, A.K., El-Essawy, F., Nassar, A.A., and El-Samanody, E.A., Synthesis, spectral, thermal and antimicrobial studies on cobalt(II), nickel(II), copper(II), zinc(II) and palladium(II) complexes containing thiosemicarbazone ligand, *J. Mol. Struct.*, 2018, vol. 1157, p. 381.